*SUPPORTING INFORMATION*

# Enhancing FRET biosensing beyond 10 nm with photon avalanche nanoparticles

Artur Bednarkiewicz[1*], Emory Chan[2] , Katarzyna Prorok[1]

1. Institute of Low Temperature and Structure Research, Polish Academy of Sciences, Okólna 2, 50-422 Wroclaw, Poland
2. The Molecular Foundry, Lawrence Berkeley National Laboratory, Berkeley, CA 94720, USA

## S1. FRET formalism

The Förster energy transfer efficiency $\eta_{FRET}$ relationship between D and A molecules staying at distance *r* is quantified as:

$$\eta_{FRET}(r) = \left[1 + \left(\frac{r}{R_0}\right)^6\right]^{-1} \quad \text{Eq.S1.}$$

The Förster distance $R_0$ is defined as a distance between D and A molecules, for which the RET efficiency drops to $\eta_{FRET}(R_0)$=50%:

$$R_0^6 = \frac{20.7}{128 \cdot \pi^5 \cdot N_A} \cdot \frac{\kappa^2 \cdot Q_D}{n^4} \cdot \frac{\int f_D(\lambda) \cdot \varepsilon_A(\lambda) \cdot \lambda^4 \delta\lambda}{\int f_D(\lambda) \delta\lambda} \quad \text{Eq.S2.}$$

where $Q_D$ is fluorescence quantum yield of the D in the absence of A, *n* is refractive index, $N_A$ is Avogadro's number, $f_D$ is the donor emission spectrum, $\varepsilon_A$ is acceptor molar extinction coefficient and k is orientation factor ($0 \leq \kappa^2 \leq 4$, $\kappa$ =2/3 is often assumed for randomly oriented D-A pairs).

**S2. The rate-equation model**

Based on the energy levels in $Nd^{3+}$, we have developed a set of rate-equations, which describe the averaged behavior of the system

$$\frac{\partial n_0}{\partial t} = W_{NR} \cdot n_1 + \frac{\frac{\beta_9 \cdot n_4}{2}}{\tau_{Nd}} - W_{CR} \cdot n_0 \cdot n_4 - W_{AT} \cdot n_0 \cdot exp\left(\frac{-\Delta E}{k \cdot T}\right) + \frac{W_{DA} \cdot n_4}{1 + \left(r/R_0\right)^6} \quad \text{Eq.S3}$$

$$\frac{\partial n_1}{\partial t} = W_{NR} \cdot \left(n_2 - n_1\right) - \frac{\sigma_{1064}^{ESA} \cdot I_{EXC}}{h\nu} \cdot n_1 + \frac{\frac{\beta_{11} \cdot n_4}{2}}{\tau_{Nd}} + W_{AT} \cdot n_0 \cdot exp\left(\frac{-\Delta E}{k \cdot T}\right)$$

Eq.S4

$$\frac{\partial n_2}{\partial t} = W_{NR} \cdot \left(n_3 - n_2\right) + \frac{\beta_{13/2} \cdot n_4}{\tau_{Nd}} \quad \text{Eq.S5}$$

$$\frac{\partial n_3}{\partial t} = 2 \cdot W_{CR} \cdot n_0 n_4 - W_{NR} \cdot n_3 + \frac{\beta_{15/2} \cdot n_4}{\tau_{Nd}}$$

Eq.S6

$$\frac{\partial n_4}{\partial t} = \frac{\sigma_{1064}^{ESA} \cdot I_P}{h\nu} \cdot n_1 - W_{CR} \cdot n_0 n_4 - \frac{n_4}{\tau_{Nd}} - \frac{W_{DA} \cdot n_4}{1 + \left(r/R_0\right)^6}$$

Eq.S7

$$\sum_{J' = \frac{9}{2};\frac{11}{2};\frac{13}{2};\frac{15}{2}} \beta_{J'} = 1; \quad \sum_{i = 0..4} n_i = 1; \quad \text{Eq.S8}$$

equations marked by gray background, indicate thermal population of $^4I_{11/2}$ in respect to the ground $^4I_{9/2}$ level. The equations marked by cyan background, indicate quenching terms, which occurs due to presence of appropriate quencher at distance r from the surface of the NP. Because these rate equations can be solved analytically only for low excitation regime, we have decided to solve them numerically. The following phenomenological parameters have been set:

1. Rate of non-radiative transitions ($W_{NR}=1/10^{-5}$ $s^{-1}$) – this parameter is characteristic for a given host material.
2. Rate of cross-relaxation ($W_{CR}=1/10^{-5}$ $s^{-1}$ ) – this parameter is proportional to the concentration of $Nd^{3+}$ ions. Lanthanides are susceptible to concentration quenching, whose origin is the cross relaxation process between neighbor lanthanides. This process is highly undesired for conventional luminescence, but important for PA mode, as it doubles the population of the first excited level. The rate of emission in lanthanides takes typical values of 1/10us – 1/500us – i.e. $1\cdot10^5$-$2\cdot10^3$, which are the inverse of their luminescence lifetimes. We have previously experimentally verified the concentration quenching mechanism in $Nd^{3+}$ doped $NaYF_4$ nanoparticles, and we noticed that c.a. 5% of $Nd^{3+}$ leads to reducing the radiative luminescence lifetimes by $2^1$. Because, at 5% of $Nd^{3+}$ the experimental lifetime equals 150 us, while theoretical lifetime equals 291 us, this means the CR rate should equal c.a. (1/150 μs – 1/290 μs) = 3200 $s^{-1}$. Using 5% of $Nd^{3+}$, may therefore be not sufficient to get PA, and larger concentrations may be required. For example for 20%, the non-radiative rate is then equal (1/11μs-1/290 μs)=87460 $s^{-1}$, which is close to the assumed $W_{CR}$ value. Therefore, we expect a concentration of around 11 % (with it corresponding $W_{CR}=10^5$ $s^{-1}$ value) should be optimal to get PA in $Nd^{3+}$ doped nanoparticles. Lower $W_{CR}$ should lead to insufficient looping.
3. Variable intensity of photoexcitation ($I_{EXC}$ from $1\cdot10^4$ to $1\cdot10^6$), where the pumping rate is defined by the absorption cross section $\sigma_{1064}^{ESA}$and pumping intensity $I_P$ at hν=1064 nm and.
4. Photoexcitation pulse width (s) – setting reasonably long photoexcitation pulse, enables to find the steady-state intensity.
5. Energy gap (ΔE = 1900 $cm^{-1}$) – this energy gap is energy difference between highest Stark level of the ground $^4I_{9/2}$ state and lowest stark level of the $^4I_{11/2}$ level.
6. All in silico experiments were performed at 42 $^oC$. Grey part of the equations correspond to thermal initial population of the first $^4I_{11/2}$ excited state, which shall contribute to photon avalanche threshold.
7. Green part of the rate equations corresponds to non-radiative energy transfer between $Nd^{3+}$ ions and appropriate acceptor molecule at distance r. In the first approximation, no particular D-A pair is considered, but $R_o$ was arbitrarily fixed to reasonable values

($R_o$<8nm). $W_{DA}$ is the rate of RET process, which is dependent on the spectral overlap between D and A molecules and concentration of A and D.

All other parameters have their typical meaning: h-Planck constant, k=Boltzmann factor, $\beta_{J'}$ (J'=9/2,11/2,13/2,15/2) are branching ratios (see below). First, the transients were calculated for $n_0$ to $n_4$ levels. To evaluate steady-state emission intensity, the photoexcitation pulse was fixed long enough to get saturation (Fig.S1, $I_{SS}$) in transient of the population $n_4$, i.e. $I(t) \sim n_4 = fun(I_{EXC}, W_{NR}, W_{CR}, \Delta E, T, t_{PULSE}, t)$. In a similar way the half-rise times were calculated $I(t_{1/2}) = ½ \cdot I_{SS}$. The variability of these factors were subsequently presented as a function of excitation intensity ($I_P$), non-radiative ($1/W_{NR}$) and cross-relaxation ($1/W_{CR}$) rates.

Based on Judd-Ofelt theory the Einstein coefficient (radiative rates) is proportional to line strength of electron-dipole transition, which is expressed as:

$$A_{ij} \sim s_{JJ'}^{ed} \sum_{\lambda = 2,4,6} \Omega_\lambda \cdot \left| \left\langle 4f^N \alpha [SL] J \middle\| U^{(\lambda)} \middle\| 4f^N \alpha' [S'L'] J' \right\rangle \right|^2 \qquad \text{Eq.9}$$

The $\langle\|U^{(\lambda)}\|\rangle$ is reduced matrix elements of the irreducible tensor operators, which indicates theoretical probability of transition between SLJ and S'L'J manifolds and the [$\Omega_2$ $\Omega_4$ $\Omega_6$ ] are intensity parameters characteristic for given ion in given matrix. Taking into account the [$\Omega_2$ $\Omega_4$ $\Omega_6$ ] = [6.07 3.05 10.52] Judd-Ofelt parameters for e.g. fluorides as well as reduced tensor [$U_2$ $U_4$ $U_6$] = [ 0.001 0.2371 0.3972] for $^4I_{9/2} \rightarrow {}^4F_{5/2}$ at ~808 nm (which is typically used to pump Nd based lasers), and [$U_2$ $U_4$ $U_6$] = [0.0000 0.1136 0.4104] for $^4I_{11/2} \rightarrow {}^4F_{3/2}$ at ~1064 nm (which is typically used as laser emission), one may calculate electric dipole oscillator strength $s^{ed}_{4I9/2 \rightarrow 4F5/2}$ (808 nm)= $4.907769 \cdot 10^{-20}$ $cm^2$, while $s^{ed}_{4I11/2 \rightarrow 4F3/2}$ (1064nm) = $4.663888 \cdot 10^{-20}$ $cm^2$, which means, the absorption cross section of ESA should be around 95% of GSA, if only the $^4I_{11/2}$ level is fully populated. The latter σ was actually measured to be $10.75 \cdot 10^{-20}$ $cm^2$ in $Nd^{3+}$ doped $NaYF_4$ single crystals[2]. Based on E.S. Levy et al. estimations, the $\sigma_{4I9/2 \rightarrow 4F3/2}$ (1064nm) ~$1 \cdot 10^{-25}$ $cm^{-2}$. Therefore the $A_{GSA}/A_{ESA}$ ratio equals to $\sigma_{4I9/2 \rightarrow 4F3/2}$ (1064nm) / $\sigma_{4I11/2 \rightarrow 4F3/2}$ (1064nm) ~ $1 \cdot 10^{-25}$ $cm^{-2}$ / 95%·$10.75 \cdot 10^{-20}$ $cm^2$ = $0.098 \cdot 10^{-5}$ = $0.98 \cdot 10^{-4}$, which satisfy the condition $R<10^{-4}$ and thus should classify the process as photon avalanche[3,4]. It is important to mention, the Nd doped $NaYF_4$ single crystals exhibited 26%, 100% and 389% higher absorption cross section and 54%, 147% and 231% higher emission cross section than $Nd^{3+}$ doped YAG, YLF, BYF.[2] This is also in agreement with calculations made by Joubert et al[5]. The only studies on PA in $Nd^{3+}$ ions demonstrated 413 nm PA emission under 603.6 nm in

$LiYF_4$ single crystal, at temperatures <40K with lasing slope factor efficiency up to 11%. The critical parameter R has reached $1.7 \cdot 10^{-4}$ for avalanche at T  40 K[5,6].

Not too much information can be found on non-radiative rates, which in fact determine the balance between non-radiative losses and looping, which is a fundamental requirement for PA to occur. In $Nd^{3+}$, the energy gap between $^4I_{15/2}$, $^4I_{13/2}$ and $^4I_{11/2}$ and the ground $^4I_{9/2}$ state are equal to around 1540, 1700 and 1480 $cm^{-1}$ respectively, with $W_{NR}$ ~$10^3$-$10^4$ $s^{-1}$ (based on $LaF_3$ host[7]). Such $W_{NR}$ corresponds to $A_{NR}$ ~ $10^{-3}$-$10^{-4}$ s, which, according to Fig.S2, makes the presented system closer to looping rather than PA. The $W_{NR}$ has a tremendous impact on the PA behavior in $Nd^{3+}$ (as shown in Fig.S2b,d), because this mechanism is present and necessary both to get looping, and simultaneously deplete the $^4I_{11/2}$ level. However, based on data available in the literature and the energy gap law, it is impossible to get univocal and reliable values for other hosts such as $NaYF_4$ (see discussion in chapter 4.2 in Crystalline Lasers: Physical Processes and Operating Schemes, Alexander Kaminskii). We have therefore presented the performance of the studied PA system for variable $W_{NR}$ values.

**S3. The outcome of the modelling**

Based on the performed modelling a series of time resolved PA emission $I_{EMI}(t)$ traces have been obtained (Fig.S1) for variable excitation intensity as a function of e.g. cross-relaxation, non-radiative rates or other phenomenological factors. These profiles enable to define quantities, further used to measure the performance of PA phenomenon, i.e. steady-state emission intensity ($I_{SS}$= $I_{EMI}(t\rightarrow\infty)$), half-rise times ($t_{1/2}$, a time from switching the photoexcitation light on, which leads to reaching half the maximal PA emission intensity $I_{EMI}(t_{1/2}) = ½\ I_{SS}$). Moreover, time points ($t_1$ and $t_2$) have been arbitrarily defined, which enable to measure the photon counts of the so called “late photons”, to quantify exclusively photons originating from PA process. As indicated later, close to PA threshold, up to PA saturation, a critical slowing down of PA emission occurrence has been experimentally shown. Therefore, PA “late photons” are quantified as $I_{LATE} = I_{EMI}(t_2) – I_{EMI}(t_1)$.

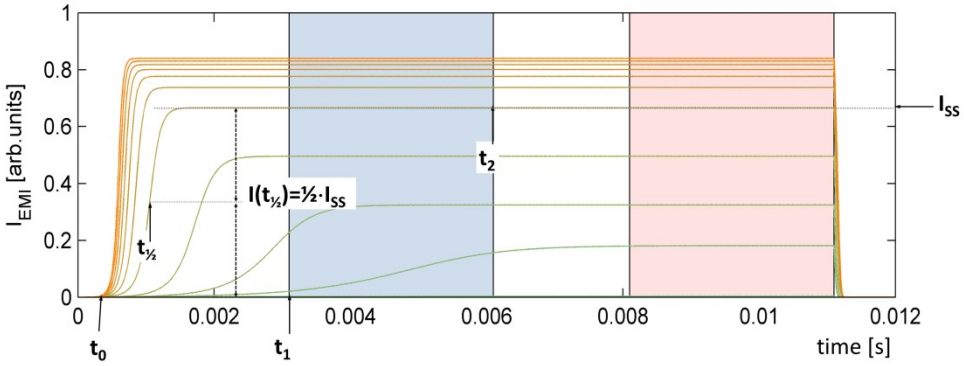


**Figure S1.** The PA luminescence rise-times for rising (green-to-orange) photoexcitation intensity.

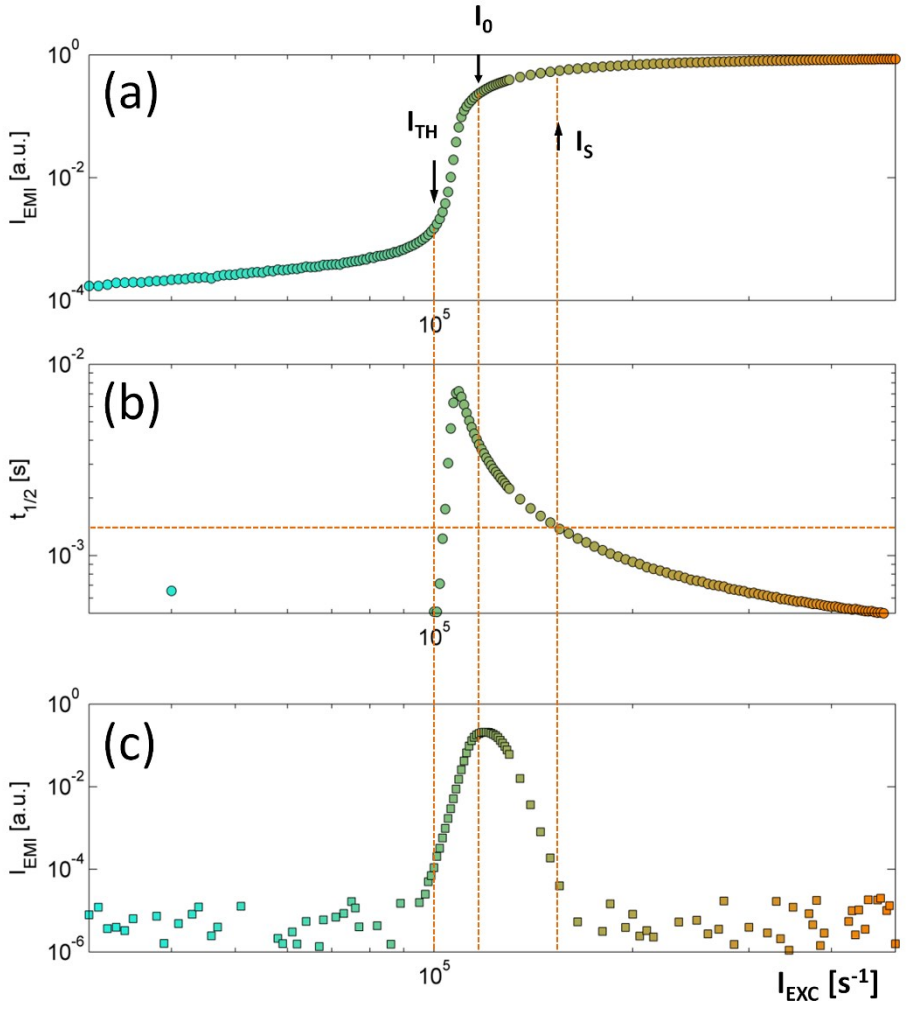


**Figure S2. The fluorescence properties of PA phenomenon.** (a) Typical "S" shape relationship, between excitation ($I_{EXC}$) and emission ($I_{EMI}$) intensities, (b) half-risetime of PA emission intensity, (c) "late" photons, indicating the photons originating from donor ions, working in a PA mode.

More details on how the $I_{SS}$ and $t_{1/2}$ were calculated can be found in Ref.[8].

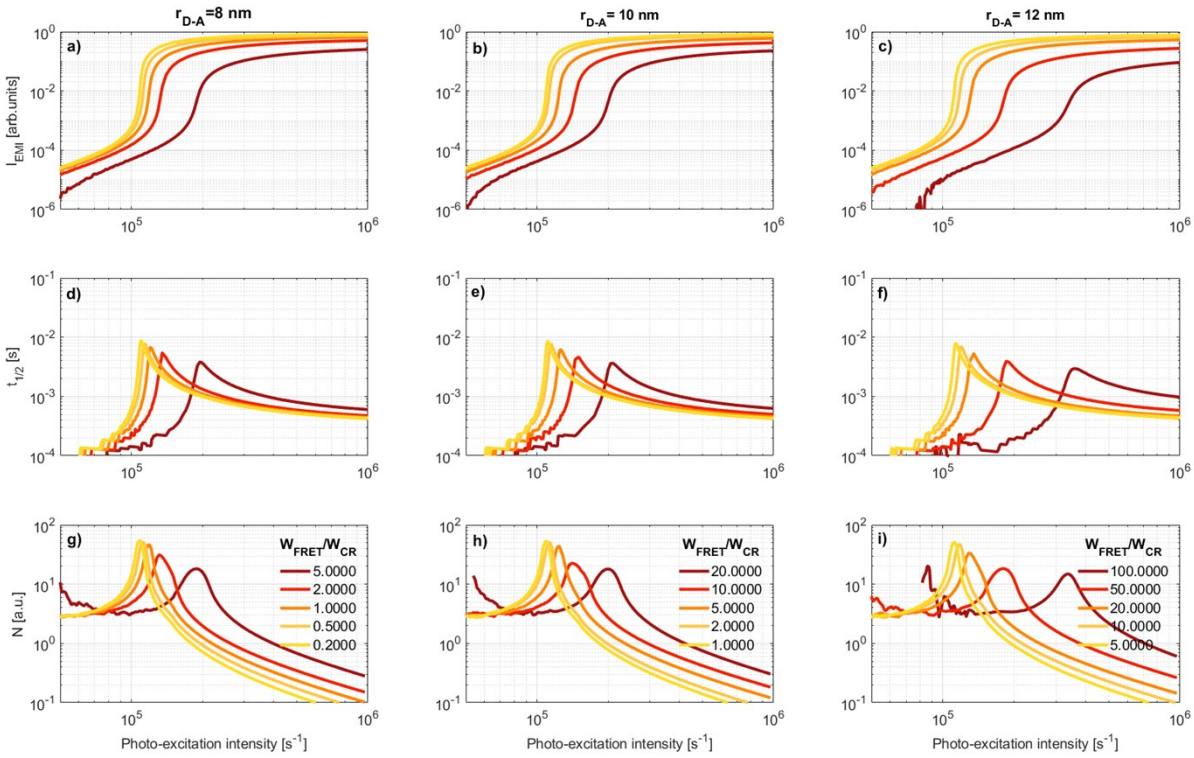


**Figure S3. Photon avalanche behavior for various distance (r) and concentration of acceptor [A].** 'S' shape power-dependence (first row), half-rise time (second row) and PA order number N (third row) are shown for donor-acceptor distance equal 8 nm (first column), 10 nm (second column) and 12 nm (third column), for variable concentration (yellow to red) of acceptor [A]. Please note that while corresponding axes ranges are identical, the [A] between data for different $r_{DA}$ is different. The parameters used for simulation: $R_o$=5 nm, $W_{CR}$=1·10$^5$, $W_{NR}$=1·10$^5$, T=32$^o$C.

## S4. Enhanced FRET behavior

Both, steady-state PA emission intensity (top row of Figure S4) as well as half rise-times (bottom row of Figure S4) depend of the concentration of acceptor-quencher molecules (measured as C = $A_{CR}/A_{FRET}$) and the distance between donors and acceptors/quenchers (Fig.S4a and d, respectively). These data are the ratio of PA intensity in coupled D-A pair normalized to PA intensity in D only NPs ($I_{DA}/I_D$). Alternatively, the corresponding half rise-times of D in a coupled D-A pair were normalized to half rise-time of D only ($\tau_{1/2\text{-}DA}/\tau_{1/2\text{-}D}$). The graphs Fig.S4b) and e) show the $I_{DA}/I_D$ for rising concentration of Q

components at fixed distances between D-A. Moreover, a 3D maps were created, showing all the three relationships, i.e. $I_{DA}/I_D$ (y axis) in respect to the concentration of A (measured as $A_{CR}/A_{FRET}$ [arb.units]) vs. distance (x distance [nm])

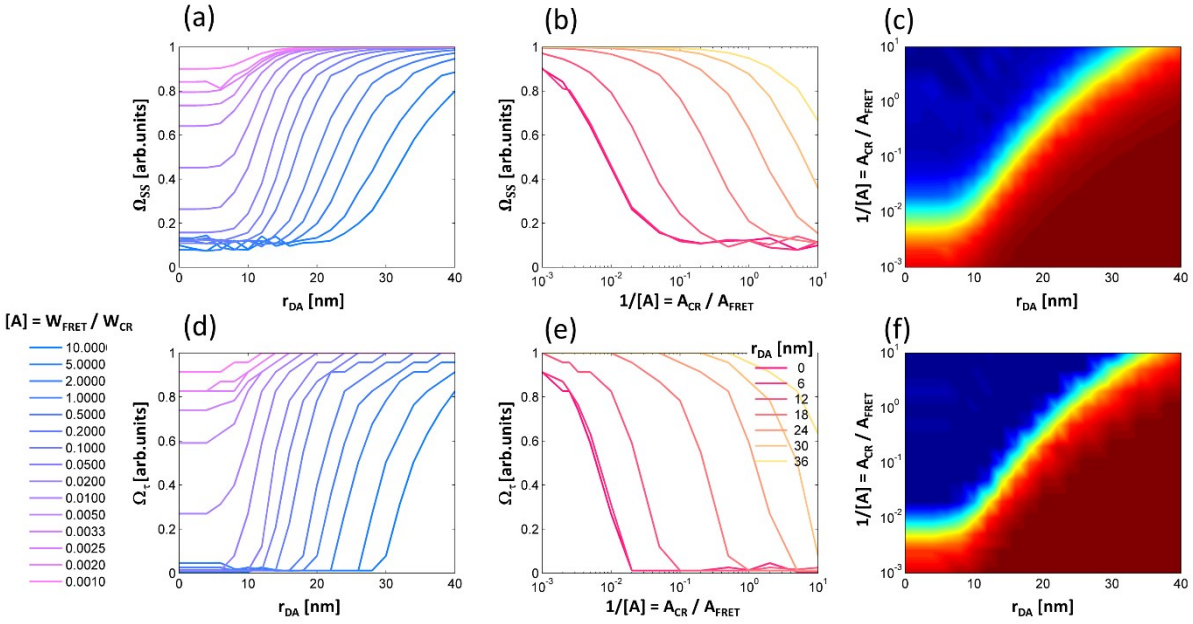


**Figure S4. The performance of eFRET system quantified by intensity (top) or half-rise times (bottom) of the D coupled to A, normalized to the respective values of the D alone.** Panels (a) and (d) show the performance of the system at different concentrations of acceptor-quencher molecules (pink to blue) at various distances between D-A species (X axis). Panels (b) and (e) show the performance of the system at different at various distances between D-A species (l=0,6,12,18,24,30,36nm) for variable concentration of acceptor (X axis). Panels (c) and (f) present combined relationship maps in respect to D-A distance (X axis) and A concentration (Y axis).

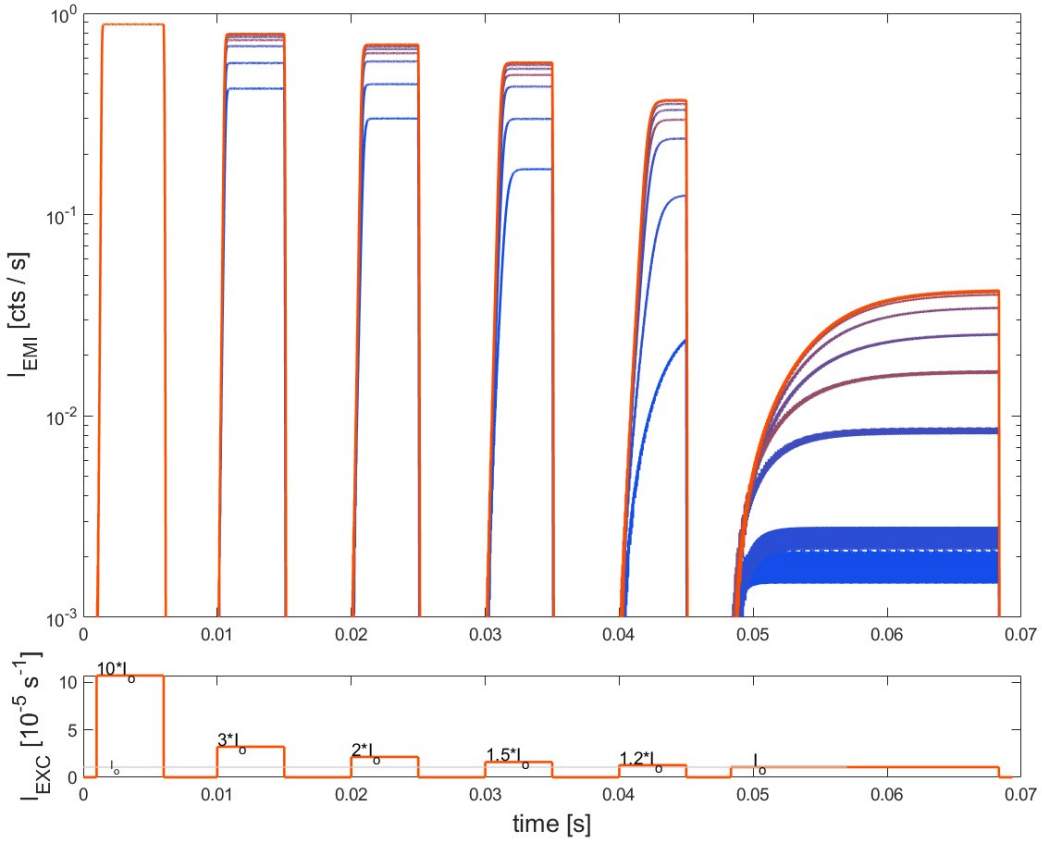


**Figure S5. Simulations of Stokes and PA anti-Stokes emission combined in the same PA nanoparticle.** The kinetics of the same PA NPs luminescence intensity (the emission from $^4F_{3/2}$, $n^4_{Nd}$ level at $\lambda_{LUM}$=860 nm) under ESA ($\lambda_{EXC}$= 1064nm) photoexcitation for variable concentrations of acceptor (blue to orange) at decreasing excitation intensity expressed in relation to $I_o$ =1.07e5. In the model, $W_{CR}$=1e5, $W_{LRET}$=1/$A_{LRET}$, where $A_{LRET}$=($1\cdot10^{-5}$ (blue), $2\cdot10^{-5}$, $5\cdot10^{-5}$, $1\cdot10^{-4}$, $2\cdot10^{-4}$, $5\cdot10^{-4}$, $1\cdot10^{-3}$, $2\cdot10^{-3}$, $5\cdot10^{-3}$, $1\cdot10^{-2}$, $2\cdot10^{-2}$, $5\cdot10^{-2}$ (orange)), $R_o$=10 nm, $R_{DA}$=15 nm.

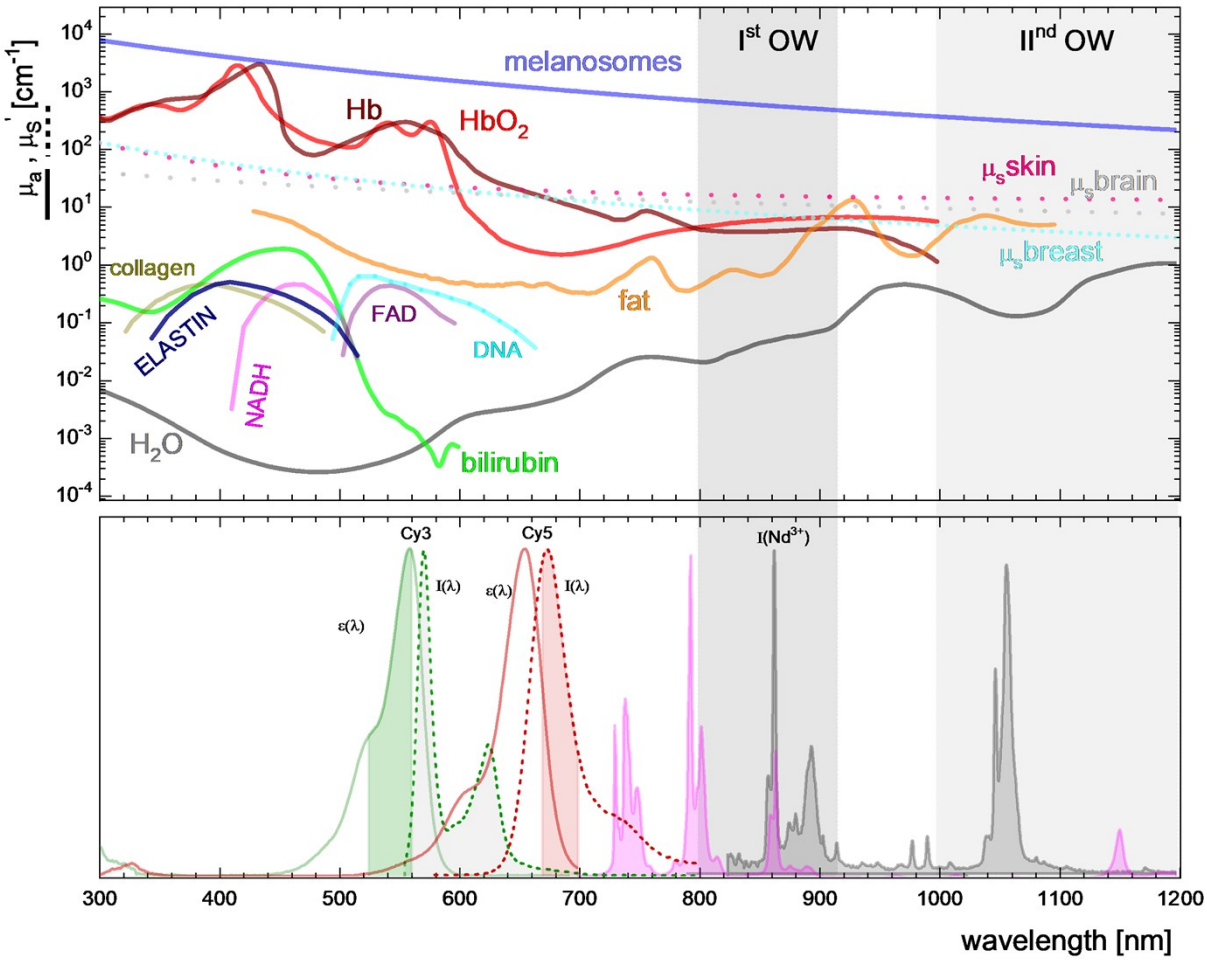


**Figure S6. Spectral properties of the $Nd^{3+}$ based PA nanoparticles as compared to tissue spectroscopy and conventional FRET organic pairs (Cy3-Cy5)**

## Supporting information references


1. Bednarkiewicz, A., Wawrzynczyk, D., Nyk, M. & Strek, W. Synthesis and spectral properties of colloidal $Nd^{3+}$doped NaYF<inf>4</inf>nanocrystals. *Opt. Mater. (Amst).* **33**, (2011).

2. Peterson, R. & Cassanho, A. Evaluation of Nd:NYF as a new laser material. in *Advanced Solid-State Lasers* TuB7 (Optical Society of America, 2001). doi:10.1364/ASSL.2001.TuB7

3. Seto, D. *et al.* Nanoscale optical thermometry using a time-correlated single-photon counting in an illumination-collection mode. *Appl. Phys. Lett.* **110**, (2017).

4. Joubert, M.-F. Photon avalanche upconversion in rare earth laser materials. *Opt. Mater. (Amst).* **11**, 181–203 (1999).

5. Joubert, M. F., Guy, S. & Jacquier, B. Model of the photon-avalanche effect. *Phys. Rev. B* **48**, 10031–10037 (1993).

6. Macfarlane, R. M. Inhomogeneous broadening of spectral lines in doped insulators. *J. Lumin.* **45**, 1–5 (1990).

7. E., P. Y. & A., K. A. Nonradiative Transitions of the Trivalent Lanthanides in Insulating Laser Crystals. *Phys. status solidi* **132**, 11–40 (2018).

8. Bednarkiewicz, A., Chan, E. M., Kotulska, A., Marciniak, L. & Prorok, K. Photon avalanche in lanthanide doped nanoparticles for biomedical applications: super-resolution imaging. *Nanoscale Horizons* **4**, 881–889 (2019).